Journal of Magnetism and Magnetic Materials 539 (2021) 168343

Contents lists available at ScienceDirect

Journal of Magnetism and Magnetic Materials

journal homepage: www.elsevier.com/locate/jmmm

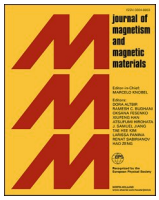

Research articles

Uncompensated magnetic moment and surface and size effects in few-nanometer antiferromagnetic NiO particles

D.A. Balaev [a,b,*], A.A. Krasikov [a], S.I. Popkov [a], S.V. Semenov [a,b], M.N. Volochaev [a], D. A. Velikanov [a], V.L. Kirillov [c], O.N. Martyanov [c]

[a] Kirensky Institute of Physics, Federal Research Center "Krasnoyarsk Scientific Center", Siberian Branch, Russian Academy of Sciences, Krasnoyarsk 660036, Russia
[b] Siberian Federal University, Krasnoyarsk 660041, Russia
[c] Boreskov Institute of Catalysis, Siberian Branch, Russian Academy of Sciences, Novosibirsk 630090, Russia

ARTICLE INFO

Keywords:
Antiferromagnetic NiO nanoparticles
Uncompensated magnetic moment
Superparamagnetism
Surface magnetic anisotropy

ABSTRACT

-The analysis of the M(H) magnetization curves of antiferromagnetic nanoparticles yields information about magnetic subsystems formed in these objects, which are characterized by a large fraction of surface atoms. However, in the conventionally investigated experimental magnetic field range of up to 60–90 kOe, this analysis often faces the ambiguity of distinguishing the Langevin function-simulated contribution of uncompensated magnetic moments μ_{un} of particles against the background of a linear-in-field dependence (the antiferromagnetic susceptibility and other contributions). Here, this problem has been solved using a pulsed technique, which makes it possible to significantly broaden the range of external fields in which the μ_{un} contribution approaches the saturation. Nanoparticles of a typical NiO antiferromagnet with an average size of $<d> \sim 4.5$ nm have been investigated. Based on the thorough examination of the M(H) magnetization curves measured in pulsed fields of up to 250 kOe, a model of the magnetic state of NiO nanoparticles of such a small size has been proposed. The average moment is ~130 μ_B (μ_B is the Bohr magneton) per particle, which corresponds to 60–70 decompensated spins of nickel atoms localized, according to the Néel hypothesis ($\mu_{un} \sim <d>^{3/2}$), both on the surface and in the bulk of a particle. A part of the surface spins unrelated to the antiferromagnetic core form another subsystem, which behaves as free paramagnetic atoms. Along with the antiferromagnetic core, an additional linear-in-field contribution has been detected, which is apparently related to superantiferromagnetism, i.e., the size effect inherent to small antiferromagnetic particles.

1. Introduction

Magnetic nanoparticles are interesting for applications in various fields of engineering and technology, including permanent magnets [1–4], magnetic memory [5–7], catalysis [8,9], biotechnology [10,11], and medicine (drug delivery, magnetic hyperthermia, etc.) [12–15]. Along with the small size and requirements for the narrow size distribution of nanoparticle ensembles, an important characteristic of such systems is their magnetic activity: a nanoparticle should remain a good nanomagnet. However, the well-known surface effects and structural defects often degrade the magnetic properties, as was observed, for example, in nanometer oxide ferrimagnetic materials [16–18]. In view of this, close attention is paid to the materials antiferromagnetically ordered in the bulk state. In such systems, at the transition to nanoscale particles, structural defects and uncompensated chemical bonds of surface atoms play a role fundamentally different from that in ferri- or ferromagnetic (FM) nanoparticles. If a bulk antiferromagnet is weakly magnetic, its nanoparticles in the presence of defects acquire a completely new quality in the form of an uncompensated magnetic moment. The moment per particle can attain hundreds of Bohr magnetons [19–36]. These size effects open up new possibilities for applications of antiferromagnetic (AFM) nanoparticles based on their magnetic characteristics.

In principle, the spin of a surface atom in the nonstoichiometric coordination can be considered to be a defect as compared with the AFM ordering of a bulk material. However, to form an uncompensated magnetic moment, defects of different types should occur, in the presence of which the numbers of "spin-up" and "spin-down" electrons are unequal. In fact, the FM ordering of a certain part of the magnetic moments of atoms in a particle should be implemented, while for most AFM

* Corresponding author.
E-mail address: dabalaev@iph.krasn.ru (D.A. Balaev).

https://doi.org/10.1016/j.jmmm.2021.168343
Received 17 December 2020; Received in revised form 8 June 2021; Accepted 23 July 2021
Available online 28 July 2021

spins, the order is mainly preserved (hereinafter, this main subsystem is referred to as the AFM particle core). The main sources of the formation of a new FM subsystem (uncompensated particle moment μ_{un}) can be considered to be defects, which lead to decompensation of spins in the sublattices. Based on the statistical considerations, the μ_{un} value will depend on whether the defects occur on the surface or over the entire volume of a particle. Néel showed [37] that the μ_{un} value can be estimated using the relation

$$\mu_{un} \sim \mu_{at} \cdot N_{at}^{b}. \quad (1)$$

Here, N_{at} is the number of atoms in a particle, μ_{at} is the magnetic moment of an atom, and exponent b is 1/3 when defects occur on the particle surface, 1/2 when they are localized both on the surface and in the bulk of a particle, and 2/3 at the odd number of planes with parallel spins in a particle. Although this hypothesis is purely model, Eq. (1) is widely used to analyze experimental data, since these cases can be distinguished by exponent b.

For the magnetic nanoparticles of almost all types, the bright effects induced by the behavior of surface spins [16–18,25,38–49], which can also be considered as a separate subsystem, have been widely debated. At low temperatures, a spin-glass-like state can be implemented in this subsystem [25,38–47]. The AFM nanoparticles are not an exception in a series of nanomaterials with the surface spin subsystem [25,43–49]. Here, it is important to distinguish this subsystem from the above-described FM subsystem, which determines the uncompensated magnetic moment of a particle.

Thus, three magnetic subsystems can coexist and interact in an AFM nanoparticle, which are the AFM core, the FM subsystem (μ_{un}), and the surface spin subsystem. All these subsystems contribute to the magnetic behavior of AFM nanoparticles, thereby complicating the analysis of their magnetic properties. The FM and surface spin subsystems are manifested in the magnetic measurements (in the temperature dependences of the static and dynamic susceptibility) [19,23,42–45] and other experimental examinations, including Mössbauer spectroscopy, magnetic resonance [40,48], and powder neutron diffraction studies [50,45]. In some cases, the μ_{un} value can be found from the Mössbauer spectroscopy [19,27] and magnetic resonance data [51,52]. Analysis of powder neutron diffraction on the AFM nanoparticle system allows one to determine a fraction of spins corresponding to the AFM-ordered core [45]. At the same time, the M(H) curve brings information on all the above-mentioned contributions corresponding to the magnetic subsystems in AFM nanoparticles. Consequently, the correct separation of the contributions of these subsystems to the observed magnetic properties of AFM nanoparticles is an important fundamental problem associated with possible applications, since it is the FM subsystem (μ_{un}) that, ultimately, is crucial for use of these particles as nanomagnets.

Similar to the case of ferro- and ferrimagnetic nanoparticles, the uncompensated magnetic moment of an AFM particle can be in the blocked or unblocked (superparamagnetic (SPM)) state. On the temperature scale, these states are separated by the SPM blocking temperature T_B, which is generally determined as

$$T_B = K_{eff} V / ln(\tau_m/\tau_0)\, k_B. \quad (2)$$

In this equation, K_{eff} is the effective anisotropy constant, which includes the bulk magnetic anisotropy and surface effects, V is the particle volume, τ_m is the measurement time, τ_0 is the characteristic particle relaxation time (typically ranging between 10^{-9}–10^{-3} s), and k_B is the Boltzmann constant.

At $T < T_B$, the magnetization process is mainly determined by the competition of the Zeeman energy $\boldsymbol{\mu}_{un} \cdot \boldsymbol{H}$ and the magnetic anisotropy energy $K_{eff}V$, which induces potential barriers for the uncompensated magnetic moment. This is the well-known mechanism of the hysteretic behavior of magnetization of single-domain magnetic particles [53]. In the SPM state ($T > T_B$), the thermal energy exceeds the magnetic anisotropy energy and the magnetization process is that $\boldsymbol{\mu}_{un}$ seeks to orient along $\boldsymbol{H}$. In this case, the magnetization (for the noninteracting magnetic moments) can be described by the classical Langevin function $L(\mu_{un}, H) = \coth(\mu_{un}H / kT) - 1/(\mu_{un}H/kT)$.

The magnetization curve for AFM nanoparticles can be presented in the approximate form [19–36]

$$M(H) = M_{FM}(H) + \chi_{total} \times H. \quad (3)$$

Here, $M_{FM}(H)$ is the contribution of the FM subsystem and the term $\chi_{total} \times H$ reflects the other contributions. The M(H) dependence, similar to (3), was repeatedly observed in different systems of AFM nanoparticles. This allows one to obtain the μ_{un} value by processing the experimental data in the temperature range of $T > T_B$ using the simulation of $M_{FM}(H)$ by the $L(\mu_{un},H)$ function [19–36,44,54,55]. However, there are some problems that strongly complicate this interpretation. They are as follows:

(i) The size distribution of AFM particles and, consequently, the μ_{un} distribution over their size must be taken into account; as was shown in [26,29,30,36,55], the neglect of this distribution can lead to the incorrect determination of the μ_{un} value.
(ii) The χ_{total} value in Eq. (3), according to [21–25,28–30,36,44,54,55], decreases with temperature surprisingly strongly, which needs special explanation.
(iii) In the conventionally used magnetic field range (up to 60–90 kOe), the experimental M(H) dependences *only tend* to attaining a linear portion, which is determined by the second term of Eq. (3); the results of fitting essentially depend on the maximum applied field [56,57] and can be ambiguous. For instance, the linear contribution, even in relatively strong (about 50–90 kOe) fields can be reproduced by the Langevin function at small μ_{un} values.

All the above-listed problems can be solved via a significant expansion of the range of magnetic fields used in the experiment. If, in a strong field, the experimental M(H) dependence will pass to a linear portion, then the contribution of the FM subsystem (μ_{un}) in this field will be saturated and can be unambiguously described by the Langevin function taking into account the size (or μ_{un}) distribution of particles. The temperature evolution of the χ_{total} value, with allowance for the AFM susceptibility χ_{AF} of the corresponding bulk antiferromagnet, allows us to distinguish the contribution of the surface spin subsystem, as well as the possible contribution of superantiferromagnetism [24,58].

Superantiferromagnetism (SAF) is another effect predicted by Néel [59,60] for small AFM particles. This is the finite-size effect inherent to AFM particle with an even number of ferromagnetic planes. When external field $\boldsymbol{H}$ is directed perpendicular to the easy magnetization axis (parallel to the ferromagnetically ordered planes), the spins of the edge plane turn along $\boldsymbol{H}$ stronger than the spins of the inner planes, since the extreme plane has only one neighboring plane. This obviously results in the enhancement of AFM susceptibility [59,60,24,58]. However, the noticeable susceptibility excess can be observed if particles have no more than several tens of FM-ordered planes in the diameter, i.e., a few nanometers. Despite the mentions of the SAF effect manifestation in the magnetic properties of AFM nanoparticles, we can only note two studies [24,58] in which, based on the data obtained in fields of several hundreds of kilooersted, the χ_{SAF} contribution to the magnetization curve of AFM-ordered ferritin was determined. Similar investigations for other AFM nanoparticle systems are lacking.

The aim of this study was to determine the contributions of different magnetic subsystems of AFM NiO nanoparticles using the measurements in pulsed fields of up to 250 kOe. A system of sufficiently small (4.5 nm on average) particles was chosen. In particles of this size, the fraction of surface atoms attains tens percent of the total number of atoms, which causes a great contribution of the FM and surface spin subsystems to the magnetic properties.

2. Experimental

2.1. Preparing and characterizing nanosized NiO

NiO nanoparticles were obtained by thermal decomposition of nickel oxalate. In contrast to the fabrication of 8-nm NiO nanoparticles in [61], a dispersion of the synthesized nickel oxalate in dimethyl sulfoxide in a mass ratio of 1:1 was prepared. The decomposition was performed with an increase in temperature to 400 °C for 40 min and 10-min exposure at this temperature.

The X-ray diffraction (XRD) pattern of the NiO nanoparticle sample was obtained on a Bruker D8 Advance (Germany) diffractometer (CuKα radiation, $\lambda = 1.5418$ Å (Fig. 1)). All the diffraction peaks correspond to the NiO phase (PDF no. 047–1049). The NiO cubic unit cell parameter is consistent with a reference value (sp. gr. *Fm*3.m, $a = b = c = 4.176$ Å, $\alpha = \beta = \gamma = 90^0$). The average size of the coherent scattering region of crystallites calculated from the XRD peak half-widths using the Scherrer equation was ~ 4.8 nm.

Transmission electron microscopy (TEM) investigations were carried out on a Hitachi HT7700 facility at an accelerating voltage of 100 kV. The powder diluted in alcohol was processed in an ultrasonic bath and then deposited onto a support mesh grid. Fig. 2 shows a typical TEM micrograph of the investigated sample and the size distribution histogram for NiO nanoparticles. The average size $< d >$ of NiO nanoparticles estimated from several micrographs was found to be 4.5 nm, which is consistent with the coherent scattering region obtained from the XRD data.

To obtain information about the behavior of the magnetic susceptibility of bulk NiO, a submicron particle powder of the NiO reagent of special purity grade was taken. This sample is hereinafter referred to as bulk NiO.

2.2. Measurements of the magnetic properties in different field ranges

The quasi-static magnetic measurements were performed on a vibrating sample magnetometer (VSM) [62] and a SQUID magnetometer [63] (the M(T) dependences in fields of 10 and 100 Oe). The investigated powder was admixed with paraffin. The temperature dependences of the magnetization were measured in the zero-field cooling (ZFC) mode and upon cooling in an external field (FC).

The M(H) magnetization curves in pulsed magnetic fields were measured on an original setup designed at the Kirensky Institute of Physics, Siberian Branch, Russian Academy of Sciences (Krasnoyarsk) [64]. A sample was well fixed within an inductance transducer of a pulsed magnetometer. The pulse length τ_{Pulse} was 16 ms. The inductance transducer used in the magnetization measurements consisted of coaxial compensated coils in which the sample was placed. The signal induced in the coils was amplified and recorded by a digital storage oscilloscope. The M(H) isotherms were measured in the temperature range of 80–250 K at a magnetic field pulse amplitude of up to 250 kOe. The M(H) dependences reported in Section 3 contain the data obtained using the pulsed magnetometer in fields of 0–250 kOe and the data obtained by the VSM method in fields of up to 60 kOe.

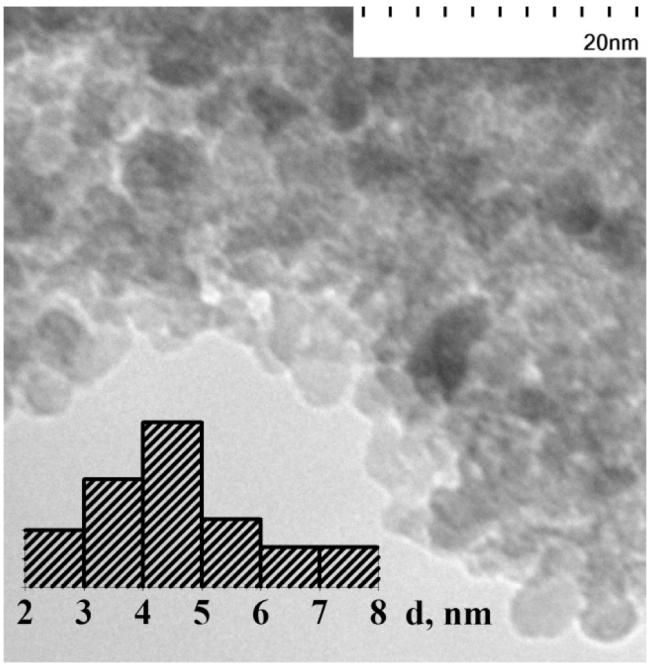

Fig. 2. TEM micrograph of nanoparticles of the investigated sample and particle size distribution histogram.

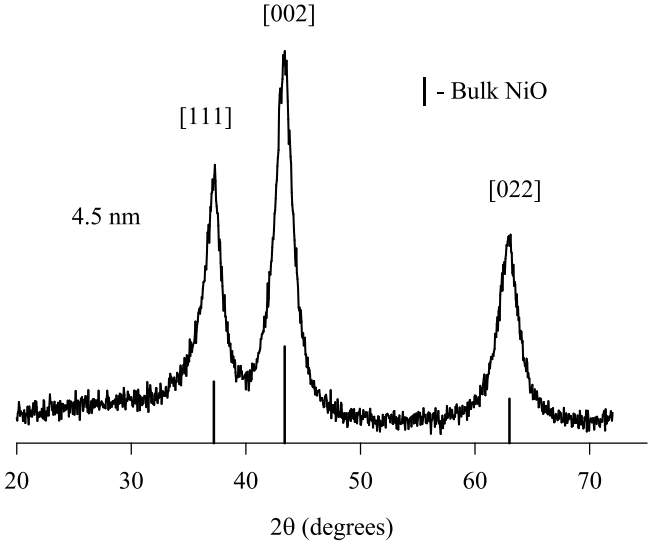

Fig. 1. XRD pattern of the investigated NiO nanoparticle sample in comparison with the line diagram illustrating the positions and relative intensities of the bulk NiO peaks.

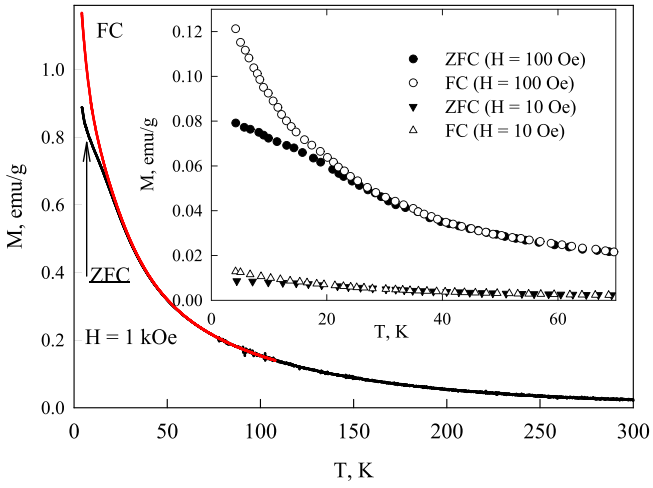

Fig. 3. Temperature dependences of magnetization for the investigated NiO sample with $< d > \approx 4.5$ nm obtained under the ZFC conditions and in the FC mode in fields of 1 kOe, 100 Oe (inset), and 10 Oe (inset).

3. Results and discussion

3.1. M(T) Dependences

Fig. 3 shows temperature dependences of the magnetization of the investigated NiO nanoparticle sample measured under the ZFC conditions and in the FC mode in magnetic fields of 1 kOe, 100 Oe, and 10 Oe. The thermomagnetic prehistory affects the M(T) behavior at temperatures below ~ 29 K. The difference between the behavior of the ZFC and FC M(T) dependences is indicative of the SPM blocking. In this case, the uncompensated magnetic moments of particles are blocked. In addition, one can see a pronounced growth of the M(T) dependences with decreasing temperature both under the ZFC and FC conditions, which is especially bright in a field of 1 kOe. This behavior is indicative of a paraprocess and evidences for the existence of isolated (or free) paramagnetic ions in the system [35,47,65–69]. In addition, it can be seen in Fig. 3 that the ZFC M(T) dependences do not contain the maximum typical of the SPM blocking, even in a weak (10 Oe) external field up to a temperature of 4.2 K. This could be interpreted as a very low SPM blocking temperature; however, in Section 3.5, we show that the allowance for the paramagnetic contribution (about 6.8% of total Ni atoms) of the surface-spin subsystem discloses a typical behavior, i.e., the presence of an M(T) maximum determined under the ZFC conditions.

3.2. Magnetization curves in different field and temperature ranges

Fig. 4 shows the M(H) dependences obtained at different temperatures in fields of up to 60 kOe. At a temperature of 4.2 K, the M(H) dependence is a hysteretic function, which is characteristic of a blocked state of the particle magnetic moments; the coercivity is ~ 0.55 kOe (see the lower inset in Fig. 4). It is noteworthy that the magnetization strongly decreases with an increase in temperature from 4.2 to 80 K. This behavior can be explained, as in the case of the M(T) dependences (see Section 3.1), by the contribution of the surface spin subsystem. At sufficiently high temperatures, this subsystem represents free paramagnetic spins and, if it passes to the spin-glass-like state, then the glass formation temperature, as a rule, is noticeably lower than the SPM blocking temperature [40–42,25,44,45]. In the investigated nanoparticles, this subsystem can be considered, approximately, to be paramagnetic; the absence of visible M(T) anomalies at low temperatures (Fig. 3) additionally confirms this fact. Below, based on the processing of the M(H) dependences in fields of up to 250 kOe, the value of this paramagnetic (PM) contribution is obtained (≈6.8% of the total number of Ni^{2+} spins, see Sec. 3.4). In addition, Fig. 4 shows the M(H) dependences corresponding to this PM contribution at T = 4.2 and 80 K. The upper inset in Fig. 4 shows the experimental M(H) dependence at T = 4.2 K obtained by subtracting the PM contribution. As expected, the resulting dependence tends to saturation.

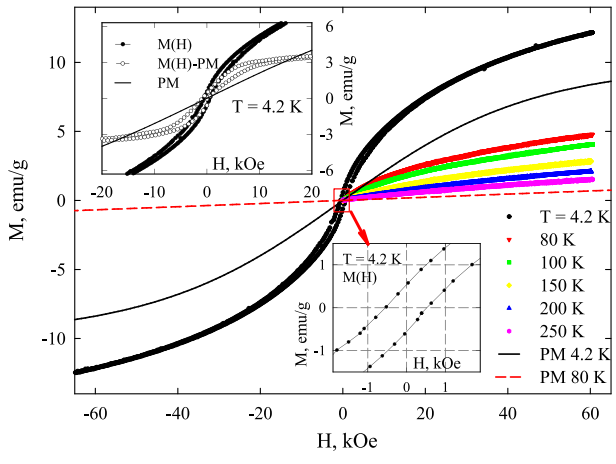

Fig. 4. Magnetization curves M(H) of the NiO nanoparticle sample obtained by the VSM technique at different temperatures (symbols). Estimated PM contribution of the surface spin subsystem at T = 4.2 and 80 K (PM) (lines). Upper inset: experimental M(H) dependence at T = 4.2 K (closed symbols) and the same dependence after subtracting the PM contribution (open symbols), as well as the PM contribution (line). Lower inset: experimental M(H) dependence at T = 4.2 K in the enlarged scale.

Fig. 5a–5d show the experimental M(H) curves (symbols) obtained for the investigated sample of NiO nanoparticles in fields of up to 250 kOe at different temperatures. In Section 3.3., we describe in detail the data processing approach used. It should be noted that the use of a pulsed technique has certain limitations caused by a decrease in the characteristic measuring time τ_m ($\tau_m \sim \tau_{Pulse}$) as compared with the standard quasi-static magnetization measurements ($\tau_m \sim 10^2$ s). As a result, in the pulsed technique, the SPM blocking temperature determined from Eq. (2) increases by ~ 50% [61]. However, for the sample under study, the T_B value is fairly small and the temperature range for measuring the M(H) dependences was above 77 K. We did not observe the M(H) hysteresis by the pulse method and the data obtained coincided with the data of the quasi-static measurements in fields of up to 60 kOe.

3.3. Processing of the M(H) dependences and mathematical background

A procedure of fitting the M(H) dependences with allowance for the distribution of magnetic moments (or the particle size distribution) contains many variable parameters, which depend on temperature. To minimize these parameters, we made several obvious assumptions. In addition, below we give some basic expressions used in the fitting procedure.

The magnetic moment μ_{un} of a particle is determined from Eq. (1) at the *b* value identical for all particles from 2 to 8 nm in size (Fig. 2). To calculate the number N_{Ni} of atoms in a particle, it is necessary to use a certain particle shape. The cubic syngony of nickel oxide suggests different possible habits of crystals, which can have the form of a cube, a complex polyhedron (dodecahedron or icosahedron), or a truncated polyhedron [70]. Since it is difficult to expect an ideal shape of small-sized crystals, it is reasonable to consider them to be truncated polyhedra with a shape close to spherical. To calculate the number N_{Ni} of nickel atoms in the particle, we used the expression $N_{Ni} \approx f \cdot \{(d/d_{Ni\text{-}Ni}) + 1\}^3$ at f = 0.52; the average distance $d_{Ni\text{-}Ni}$ between nickel atoms was taken to be ~ 0.3 nm [71].

The μ_{un} value obtained from N_{Ni} using Eq. (1) corresponds to the uncompensated moment at T = 0 K. However, similar to a decrease in the saturation magnetization of ferromagnets with an increase in temperature (the spin wave damping), the μ_{un} value depends on temperature, which was observed by many authors [19–30,36,44,54,55]. Therefore, at each temperature, the μ_{un} value was determined as

$$\mu_{un}(T) \sim \mu_{Ni} \cdot q(T) \cdot N_{Ni}^{b}. \quad (4)$$

Here, q(T) at each temperature can take some value within $q \leq 1$, q (T = 0) ≡ 1, and *b* = const.

The m(H) curve for each particle is determined by the Langevin function: $m(H, T) = L(\mu_{un}(T), H) \cdot \mu_{un}(T)$. For the sampling from $N_{P\ TEM}$ = 83 particles (the data of the histogram in Fig. 2), we obviously have M (H, T) = Σm(H, T), where the summation was made over all 83 particles detected in the TEM measurements. To pass to the specific magnetization (in emu/g units, as in the experiment), it is necessary to use the ratio between the number N_{Niperg} of Ni atoms in unit NiO mass and the number $N_{Ni\ TEM}$ of Ni atoms in the sampling of 83 particles. The number N_P of particles per sample gram will be $(N_{Niperg}/N_{Ni\ TEM}) \times N_{P\ TEM}$. The $N_{Ni\ per\ g}$ value is ~ $8 \cdot 10^{21}$ and the calculation of $N_{Ni\ TEM}$ yielded a value of ~ $2.28 \cdot 10^5$; we denote their ratio as N_P^*: $N_P^* = N_{Ni\ per\ g} / N_{Ni\ TEM}$.

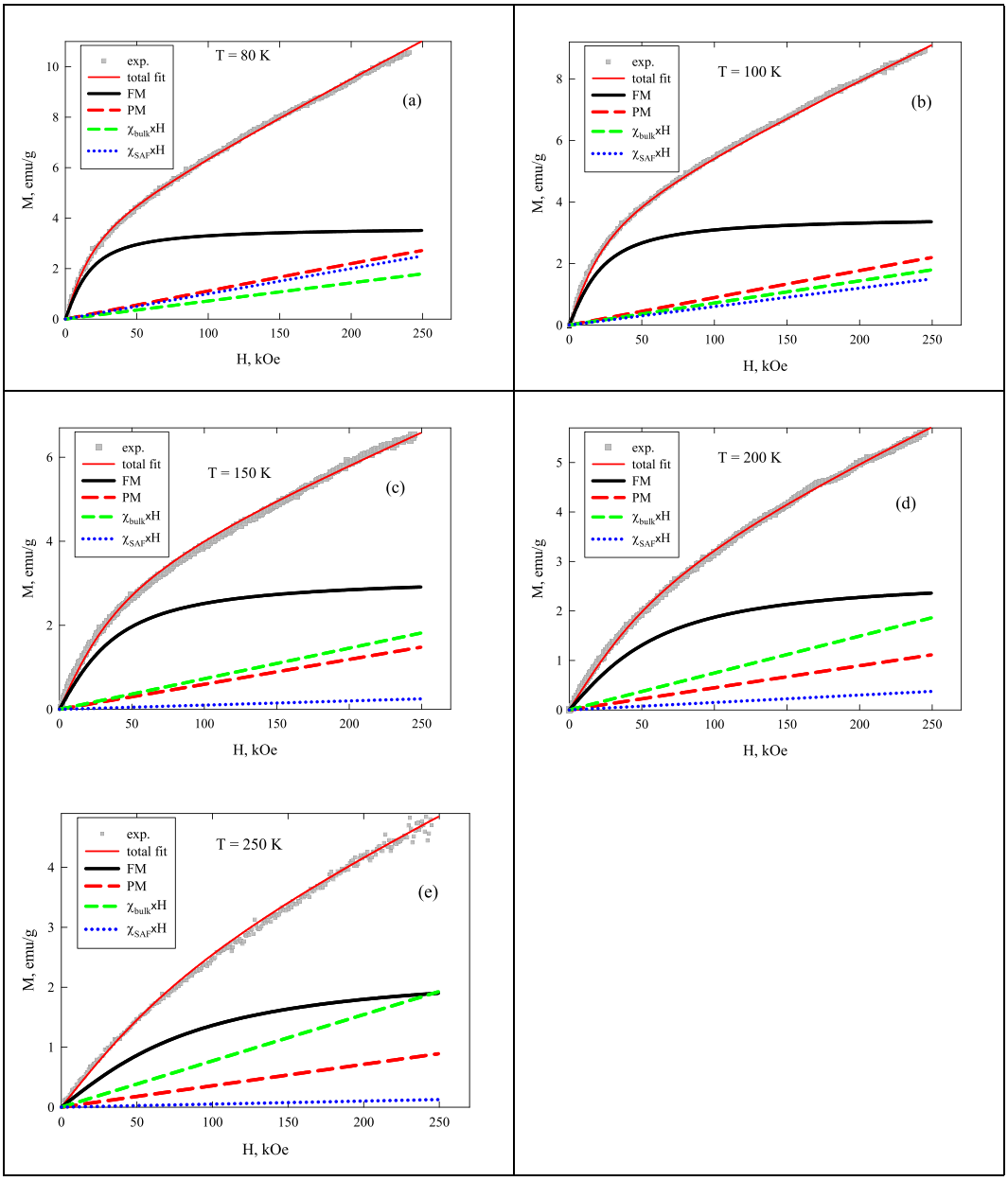

Fig. 5. Experimental magnetization curves for the NiO nanoparticle sample at different temperatures (symbols). Solid lines correspond to the best fitting using Eq. (11) (total fit) and the separate contributions of the ferromagnetic (FM) and paramagnetic (PM) subsystems, the AFM particle core $\chi_{bulk} \times H$, and the linear dependence $\chi_{SAF} \times H$ predicted by the SAF effect.

Then, the N_P^* value is 3.5 10^{16}. The fittings presented below were obtained at the N_P^* value larger by 10%, which, in our opinion, is in good qualitative agreement for a system of extremely small particles. Based on the aforesaid, we write the contribution of the uncompensated moments M_{FM} of particles in the form

$$M_{FM}(H, T) = N_P^* \cdot \Sigma L(\mu_{un}(T), H) \cdot \mu_{un}(T). \quad (5)$$

Let us make some remarks concerning the evaluation of a fraction of spins forming the FM subsystem. The number of atoms in the FM subsystem in one particle is determined, according to Néel Eq. (1), as $N_{Ni}{}^b$. Averaging of the quantity $N_{Ni}{}^b/N_{Ni}$ over the number of particles $N_{Ni\ TEM}$ will yield the $P_{FM\ Ni}$ value, i.e., a fraction of atoms forming the FM subsystem for the entire sample. The $P_{FM\ Ni}$ value can also be obtained directly from Eq. (5), taking into account that, at T = 0, the saturation magnetization M_{FM} of the FM subsystem can be determined as $N_P^* \Sigma\mu_{un}(T = 0)$. The theoretical value of saturation magnetization $M_{S\ NiO}$ of a fully polarized NiO is ~ 148 emu/g (this value is obtained for the nickel atom magnetic moment $\mu_{Ni} = 2\mu_B$). Then,

$$P_{FM\ Ni} = M_{FM}/M_{S\ NiO}. \quad (6)$$

Let us proceed to the paramagnetic contribution. This contribution can obviously be written in the form

$$M_{PM}(H, T) = M_{PM} \cdot B(\mu_{Ni}, H/k_B T) \quad (7)$$

Here, M_{PM} is the saturation magnetization of the PM contribution related to the concentration of paramagnetic nickel atoms and B(μ, H/k_BT) is the Brillouin function. To preliminary estimate the PM contribution, the dependences $\chi_{bulk} \times H$ were subtracted from the experimental M(H) dependences and the data obtained were used to determine the dM/dH values in strong fields. Then, the additive portion of the dM/dH dependence proportional to 1/T was extracted, which was seed (and preserved the functional dependence 1/T during fitting) for the PM

contribution in the further fitting. Analogously to Eq. (6), the fraction of PM atoms can be determined as

$$P_{PM\ Ni} = M_{PM}/M_{S\ NiO}. \quad (8)$$

The contribution of the AFM particle core to the magnetization is usually written as $M_{bulk}(H, T) = \chi_{bulk}(T) \times H$, where χ_{bulk} is the AFM susceptibility of the powder of submicron particles. This linear dependence is applicable if (i) there are no changes in the magnetization due to the spin flop transition and (ii) the external field does not exceed the field of the full saturation of the magnetization (the spin flip processes). The latter is undoubtedly valid as long as the exchange field in NiO (see below) is much stronger than the experimental field. Concerning the spin flop transition, despite several repots on the observed M(H) features caused by the spin flop transition in AFM nanoparticles [72,73], the experimental data presented in Figs. 4 and 5 show no anomalies that could be interpreted in this way. The absence of the spin flop transition in very small (smaller than, at least, 10 nm) AFM nanoparticles was discussed in [58,74] and attributed to the surface anisotropy effect.

To correctly take into account the AFM susceptibility, we used the $\chi_{bulk}(T)$ dependence obtained on the bulk NiO sample. However, a part of Ni magnetic moments in a nanoparticle is spent to the formation of μ_{un} (Eq. (6)) or forms the PM subsystem (Eq. (8)). Therefore, the correction of the AFM core contribution in the form of the coefficient (1 – P) is required. Here, $P = P_{FM\ Ni} + P_{PM\ Ni}$ is the total fraction of the magnetic moments of Ni atoms forming the PM and FM subsystems. Consequently, the $M_{bulk}(H, T)$ contribution corresponding to the AFM susceptibility of the bulk material of the particle core will be written as

$$M_{bulk}(H, T) = (1 - P)\cdot\chi_{bulk}(T) \times H. \quad (9)$$

Concerning the possibility of another contribution, i.e., the SAF effect, the corresponding M(H) dependence can be presented as the term $\chi_{SAF}(T) \times H$ [24,58], so the total susceptibility of an ensemble of AFM nanoparticles is $\chi_{bulk} + \chi_{SAF}$. The χ_{SAF} value depends on the particle size and on a number of outmost ferromagnetically ordered planes that are coupled weaker than those in the core. If the only plane on the particle edge is considered, then the χ_{SAF} value is the same as the χ_{bulk} one. If more than one ferromagnetically ordered planes are considered, the χ_{SAF} value can exceed the bulk susceptibility. Generally, $\chi_{SAF}(H)$ is a nonlinear dependence on the external field. It decreases very slightly when the external field does not exceed the "size-dependent" field h and, then, in strong magnetic fields, χ_{SAF} approaches zero. The value of field h depends on number N of ferromagnetically ordered planes (N is the even number) as $h = H_E/N$ [24,58], where H_E is the exchange field of an antiferromagnet. In bulk NiO, the H_E value is ~ 9700 kOe [75]. At N ~ 14–16, which corresponds to an average-size particle at an interplanar spacing of ~ 0.3 nm [71], we obtain h ~ (600–700) kOe. This value can be somewhat overestimated, since H_E is proportional to the Néel temperature, which is known to decrease for AFM nanoparticles. However, according to Sec. 3.4, a decrease in the Néel temperature is less than 20% for the sample under study; therefore, an expected decrease in H_E and h is nearly the same. Thus, the h value is about 500–550 kOe, which exceeds twice the maximum field used in our experiments (250 kOe). In view of the aforesaid, we can express the contribution of the SAF effect to the magnetization via the field-independent SAF susceptibility χ_{SAF} as

$$M_{SAF}(H, T) = \chi_{SAF}(T) \times H, \quad (10)$$

where $\chi_{SAF}(T)$ is already the fitting (if necessary) parameter.

Thus, using Eqs. (5), (7), (9), and (10), we derive the full expression for analyzing the experimental M(H) data

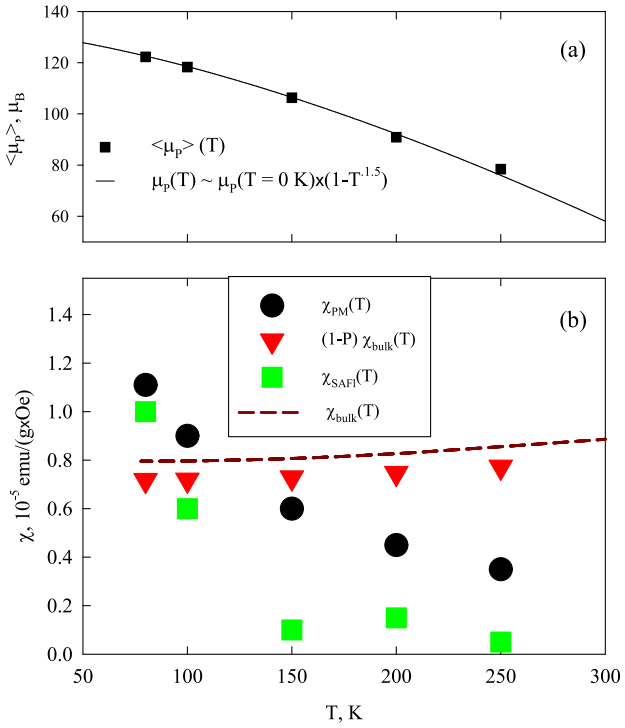

Fig. 6. Temperature dependences of (a) the average uncompensated magnetic moment of particles and (b) magnetic susceptibility χ(T) of the contributions of different magnetic subsystems (together with $\chi_{bulk}(T)$ for bulk NiO). The solid line in (a) is plotted using Eq. (12).

Eq. (11) contains only two temperature-dependent fitting parameters, q (in $\mu_{un}(T)$ – Eq. (4)) and χ_{SAF}. The b, M_{PM}, and N_P^* values remained constant at different temperatures. The lines in Fig. 5a–5e show the results of best fitting using Eq. (11) and the separated contributions of the uncompensated moments of particles (FM), the paramagnetic subsystem (PM), the AFM-ordered particle core $\chi_{bulk} \times H$, and the SAF effect $\chi_{SAF} \times H$. The best agreement was observed at $b = 0.54 \pm 0.02$, $N_P^* = (3.8 \pm 0.2) \cdot 10^{16}$, and $M_{PM} = 10 \pm 1$ emu/g. In Section 3.4., we analyze these quantities and discuss their temperature dependences.

3.4. Contributions of the magnetic subsystems and their temperature evolution

The value $<\mu_{un}>(T = 0)$ at an obtained value of $b = 0.54$ was ~ 133 μ_B; i.e., the uncompensated magnetic moment is formed by 60–70 spins of nickel atoms on average. According to the Néel hypothesis (Eq. (1)), the exponent $b = 0.54$ indicates that the spins forming the FM subsystem (or, similarly, defects leading to the formation of the FM subsystem) are located both at the surface and in the bulk of a particle. The fraction of such spins is about 3% of all nickel atoms in the NiO particle of average size ($N_{Ni} \sim 2.13 \times 10^3$ at $<d> = 4.5$ nm in the approximation of the almost spherical shape). The temperature evolution of the uncompensated moment $<\mu_{un}>$ determined by averaging over all particles $(\Sigma\mu_{un})/N_{Ni\ TEM}$ is illustrated in Fig. 6a. The obtained $<\mu_{un}>(T)$ dependence is a monotonic function, which is well described by the law

$$M_{total}(H, T) = N_P^*\Sigma L(\mu_{un}(T), H)\cdot\mu_{un}(T) + M_{PM}\cdot B(\mu_{Ni}, H/k_B T) + +(1 - P)\cdot\chi_{bulk}(T) \times H + \chi_{SAF}(T) \times H, \quad (11)$$

$$< \mu_{un} > (T) = < \mu_{un} > (T = 0) \cdot (1 - \beta T^{a}) \quad (12)$$

at **a** = 3/2. This exponent follows from the classical consideration of spin waves in a bulk ferri- and ferromagnet (the Bloch's law). Dependence (12) for the uncompensated moment of AFM nanoparticles was observed previously; the exponent **a** ranged from 3/2 to 2 [26,28,35,54].

Figure 6b illustrates the temperature evolution of the quantities $\chi_{bulk}(T)$, $(1 - P) \cdot \chi_{bulk}(T)$, $\chi_{SAF}(T)$, and $\chi_{PM}(T)$. The latter is the PM susceptibility, since the PM contribution of Ni^{2+} spins at $T \geq 80$ K and H of up to 250 kOe can be considered, with good accuracy, to be a linear field dependence. The expansion of the Brillouin function in a series yields $\chi_{PM} \approx M_{PM} \times \mu_{Ni}^{2}/3k_BT$. At temperatures of 80–100 K in a strong field, the contribution of all the magnetic subsystems is approximately the same, while at low temperatures (4–30 K), due to the dependence ~ 1/T (the paraprocess), the PM contribution becomes dominant in weak and moderate fields (Figs. 3, 4). A value of $M_{PM} = 10$ emu/g obtained by fitting was used to separate the magnetic hysteresis loop at T = 4.2 K, which corresponds to the FM subsystem (see the upper inset in Fig. 4, Section 3.2). Using a value of $M_{PM} = 10$ emu/g, we obtain from Eq. (8) a fraction of atoms forming the PM subsystem: $P_{PM\ Ni} \approx 6.8\%$ or about 150 atoms in an average-size particle. This value is noticeably smaller than the number of surface atoms, which, at $< d > = 4.5$ nm, in the spherical shape approximation, amounts to about 600, while for a cubic particle with the same size, it is about 1180. On the other hand, a cubic particle 4.5 nm in size contains about 160 atoms on the edges and this value is similar to the number of atoms forming the PM system (~150). This evidences for the fact that free spins are located mainly on the edges, protrusions, and nonuniform (convex) parts of the particle surface.

The above conclusion allows us to speak more reasonably about the presence of a noticeable SAF effect in the investigated particles. The PM subsystem consisting of isolated surface spins occupies the particle surface only in part and the atomic planes with the FM-ordered spins (at their total number being even) can remain on the particle surface. It is the main condition that is required for the SAF effect. At temperatures of 80 and 100 K, the excess susceptibility χ_{SAF} has approximately the same value as the AFM susceptibility. This doubling of the resulting susceptibility ($\chi_{SAF} + \chi_{bulk}$) relative to χ_{bulk} is typical of the SAF effect at $h < H_E$ [24,58]. Surprisingly, the χ_{SAF} value was found to rapidly decrease with temperature (Fig. 6b). Possibly, the temperature of ordering inside these edge planes is lower than in the planes inside a particle. A decrease in the Néel temperature of AFM nanoparticles was reported in many works [76–81] (see below). In the extreme planes of the spins, this decrease can be more pronounced. An increase in the susceptibility at temperatures of 80 and 100 K was determined fairly reliably, which points out the existence of a contribution caused, most likely, by the SAF effect. Note that, for the NiO samples with coarser particles ($< d > \sim 8.5$ nm), the slope of the M(H) dependences in the strong-field range was described well only by the $\chi_{bulk}(T)$ and $\chi_{PM}(T)$ contributions [35].

It is interesting to compare the temperature dependences of the saturation magnetization of the FM subsystem $M_{FM}(T)$ for the NiO samples with different particle sizes. Fig. 7 shows the $M_{FM}(T)$ dependences for the sample examined in this work and for the sample of NiO nanoparticles with an average size of 8.5 nm from [35]. In addition to the significant growth of the $M_{FM}(T)$ value with a decrease in the AFM particle size, we can observe another effect; specifically, the temperature at which the M_{FM} value tends to zero obtained by the extrapolation of the data using Eq. (12) depends on the particle size. For 8.5-nm nanoparticles, this temperature is ~ 510 K, which is close to the Néel temperature of bulk NiO (~520 K [76,81]). A decrease in the Néel temperature of AFM nanoparticles is related to the size effect [76–81]. For the sample investigated in this study ($< d > \approx 4.5$ nm), the obtained magnetic ordering temperature is already ~ 430 K. The results on the reduction of the Néel temperature of NiO nanoparticles agree well with the data reported in [76,81]. Another important fact is that the FM subsystem formed by uncompensated spins exists together with the main AFM subsystem.

3.5. SPM blocking temperature and effect of the surface magnetic anisotropy

As was mentioned in Section 3.1, the ZFC M(T) dependences do not contain the maximum typical of SPM blocking, although the difference between the FC and ZFC curves is significant (Fig. 3). Obviously, the PM contribution, which has a significant value, will additively enter the general M(T) dependence. Fig. 8 shows the M(T) dependences obtained in the ZFC mode and in the FC mode in fields of 100 Oe and 1 kOe, together with the dependences obtained by subtracting the PM contribution at $M_{PM} = 10$ emu/g. It can be seen that, after the subtracting, the $M(T)_{ZFC}$ dependences already contain characteristic maxima; the maximum position shifts toward lower temperatures with increasing field.

These corresponding maximum temperatures or blocking temperatures T_B are 8.7and 7.5 K at H = 100Oe and 1kOe, respectively.

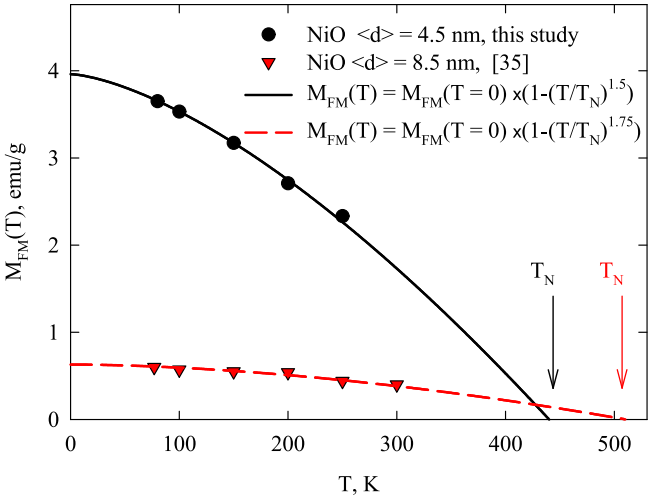

Fig. 7. Temperature dependences of the saturation magnetization of the FM subsystem $M_{FM}(T)$ for the sample investigated in this study ($< d > \approx 4.5$ nm) and the NiO nanoparticles with a size of $< d > \approx 8.5$ nm from [35]. The lines are plotted using dependence (12); the magnetic ordering temperatures obtained by the extrapolation of this dependence are indicated.

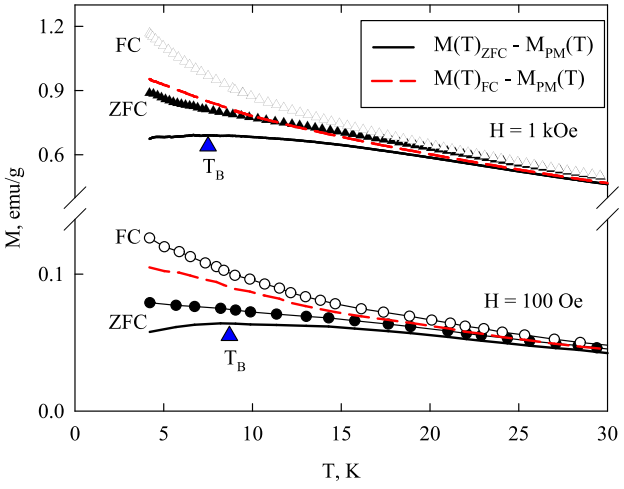

Fig. 8. FC and ZFC temperature dependences of the magnetization $M(T)_{FC}$ and $M(T)_{ZFC}$ (symbols) and the same dependences after subtracting the PM contribution (Eq. (7)) at $M_{PM} = 10$ emu/g (lines).

Assuming that T_B corresponds to the blocking of average-size particles, we obtain using Eq. (2) at typical values of $\tau_0 = 10^{-11}$s and $\tau_m \sim 10^2$s [19] that the effective magnetic anisotropy constant is K_{eff} is $\sim 3.9 \times 10^5$ erg/cm^3. Assuming that the temperature of the irreversible M(T) behavior is ~ 29 K (see Fig. 3 and Section 3.1.), which corresponds to the SP blocking of particles with a largest size (d = 8 nm), at the same τ_0 and $\tau_m$values we obtain $K_{eff} \approx 2.98 \times 10^5$erg/cm^3. These K_{eff} values are noticeably higher than the magnetic anisotropy constant $K_{bulk} = 0.8 \times 10^5$ erg/cm^3 of bulk nickel oxide [82]. This behavior frequently observed in FM nanoparticles is usually explained by the manifestation of the surface magnetic anisotropy contribution [69,82–90]. This contribution dependent on the particle size is usually written in the form $K_{eff} = K_{bulk} + 6K_S/d$, where K_S is the surface magnetic anisotropy constant [91,92]. Using this expression and the data presented above, we obtain $K_S \approx 0.026 \pm 0.003$ erg/cm^2. A significant contribution of the surface magnetic anisotropy to the magnetic properties of AFM nanoparticles was mentioned in [32,54,61,82,93–98], including the case of NiO ones [61,69,82,96–98].

4. Concluding remarks

The results of the study of the magnetic properties and analysis of the magnetization curves obtained in fields of up to 250 kOe allowed us to propose the following model of the magnetic state of AFM NiO nanoparticles with an average size of about 4.5 nm. The magnetic moment of particles, or the FM subsystem, is formed by decompensated spins due to defects located both on the surface and in the bulk of a particle (Néel relation (1) is satisfied at $b \sim 0.54$). The fraction of spins of this subsystem is about 3% or their number is 60–70, which yields an uncompensated particle moment of about 130 Bohr magnetons. In this case, the saturation magnetization M_{FM} of the FM subsystem attains 4 emu/g. The M_{FM} value monotonically decreases with temperature according to the power law $\sim (1 - (T/T_N)^a)$; i.e., the FM subsystem exists as long as there is the AFM ordering in a particle.

A part of the surface spins is not exchange-coupled with the AFM core and exhibits the paramagnetic behavior in a wide temperature range, while the sample under study shows no obvious signs of the transition to the spin-glass state up to a temperature of 4.2 K. The fraction of these free spins is about 7% of the number of nickel atoms in a particle, which is much less than the fraction of surface atoms. This fact indicates that free (exchange-uncoupled) spins are located mainly on the faces or convex parts of the particle surface. This PM subsystem makes a noticeable additive contribution to the magnetic behavior of nanoparticles in a wide temperature range, especially at low temperatures.

The AFM ordering is preserved almost over the entire particle volume; it covers about 90% of the spins of nickel atoms. Along with the field-linear contribution of the AFM particle core (taking into account the spins spent to the formation of the FM and PM subsystems), there is a noticeable increase in the susceptibility, which can be explained by the SAF effect.

Although the ZFC temperature dependence of magnetization M(T) reveals no extrema, the account for the contribution of the PM subsystem allowed us to find a pronounced maximum in the ZFC M(T) dependence. This maximum ($T_B \approx 7.5$ K) corresponds to the SPM blocking of the uncompensated magnetic moments. Using classical Néel-Brown expression (2) and the blocking temperatures (both T_B and the bifurcation temperature of the FC and ZFC M(T) dependences), the effective magnetic anisotropy constant K_{eff} was obtained. The K_{eff} value is noticeably higher than the bulk magnetic anisotropy constant of NiO. It is reasonable to attribute this to the surface magnetic anisotropy contribution; the corresponding constant K_S is ~ 0.026 erg/cm^2. The results obtained demonstrate a significant role of defects and surface effects in the formation of the magnetic state of AFM nanoparticles.

CRediT authorship contribution statement

D.A. Balaev: Conceptualization, Methodology, Formal analysis, Writing - original draft. **A.A. Krasikov:** Investigation, Software, Formal analysis. **S.I. Popkov:** Investigation, Validation. **S.V. Semenov:** Investigation, Validation. **M.N. Volochaev:** Investigation, Validation. **D.A. Velikanov:** Investigation, Validation. **V.L. Kirillov:** Resources, Validation. **O.N. Martyanov:** Resources, Writing - review & editing.

Declaration of Competing Interest

The authors declare that they have no known competing financial interests or personal relationships that could have appeared to influence the work reported in this paper.

Acknowledgments

The TEM study was carried out on the equipment of the Krasnoyarsk Territorial Center for Collective Use, Krasnoyarsk Scientific Center, Siberian Branch, Russian Academy of Sciences.

References.

[1] A. López-Ortega, E. Lottini, C. de Julian Fernández, S. C., Exploring the magnetic properties of cobalt-ferrite nanoparticles for the development of rare-earth-free permanent magnet, Chemistry of Materials 27 (2015) 4048-4056. doi:10.1021/acs.chemmater.5b01034.
[2] F.J. Pedrosa, J. Rial, K. M. Golasinski, M. N. Guzik, A. Quesada, J. F. Fernández, J. Deledda S., Camarero, A. Bollero, Towards high performance CoFe2O4 isotropic nanocrystalline powder for permanent magnet applications, Applied Physics Letters 109, 223105(2016). doi:10.1063/1.4969064.
[3] S. Ohkoshi, A. Namai, T. Yamaoka, M. Yoshikiyo, K. Imoto, T. Nasu, S. Anan, Y. Umeta, K. Nakagawa, H. Tokoro, Scientific Reports 6, 27212 (2016).| DOI: 10.1038/srep27212.
[4] S.S. Yakushkin, D.A. Balaev, A.A. Dubrovskiy, S.V. Semenov, Y.V. Knyazev, O. A. Bayukov, V.L. Kirillov, R.D. Ivantsov, I.S. Edelman, O.N. Martyanov, Ceram. Int. 44 (2018) 17852.
[5] S. Singamaneni, V.N. Bliznyuk, C. Binek, E.Y. Tsymbal, J. Mater. Chem. 21 (2011) 16819.
[6] K.K. Kefeni, T.A.M. Msagati, B.B. Mamba, Mater. Sci. Eng. **B** 215 (2017) 37–55.
[7] S. Ohkoshi, A. Namai, M. Yoshikiyo, K. Imoto, K. Tamazaki, K. Matsuno, O. Inoue, T. Ide, K. Masada, M. Goto, T. Goto, T. Yoshida, T. Miyazaki, Angew. Chem. 128 (2016) 1–5.
[8] Q. Zhang, X. Yang, J. Guan, ACS Appl. Nano Mater. 2 (2019) 4681–4697.
[9] T. Nowitzki, A.F. Carlsson, O. Martyanov, M. Naschitzki, V. Zielasek, T. Risse, M. Schmal, H.-J. Freund, M. Baümer, J. Phys. Chem. **C** 111 (2007) 8566–8572.
[10] S.Y. Srinivasan, K.M. Paknikar, D. Bodas, V. Gajbhiye, Nanomedicine 13 (2018) 1221–1238, https://doi.org/10.2217/nnm-2017-0379.
[11] T. Wang, Z. Jiang, T. An, G. Li, H. Zhao, P.K. Wong, Environ. Sci. Technol. 52 (2018) 4774–4784, https://doi.org/10.1021/acs.est.7b06537.
[12] S. Amiri, H. Shokrollahi, The role of cobalt ferrite magnetic nanoparticles in medical science, Mater. Sci. Eng. C 33 (1) (2013) 1–8, https://doi.org/10.1016/j.msec.2012.09.003.
[13] K. Dobretsov, S. Stolyar, A. Lopatin, Acta Otorhinolaryngol. Ital. 35 (2) (2015) 97–102.
[14] T. Yadavalli, H. Jain, G. Chandrasekharan, R. Chennakesavulu, AIP Adv. 6 (2016), 055904, https://doi.org/10.1063/1.4942951.
[15] S.V. Stolyar, D.A. Balaev, V.P. Ladygina, A.A. Dubrovskiy, A.A. Krasikov, S. I. Popkov, O.A. Bayukov, Y.V. Knyazev, R.N. Yaroslavtsev, M.N. Volochaev, R. S. Iskhakov, K.G. Dobretsov, E.V. Morozov, O.V. Falaleev, E.V. Inzhevatkin, O. A. Kolenchukova, I.A. Chizhova, J. Supercond. Nov. Magn. 31 (2018) 2297.
[16] A. Millan, A. Urtizberea, N.J.O. Silva, F. Palacio, V.S. Amaral, E. Snoeck, V. Serin, J. Magn. Magn. Mater. 312 (2007) L5.
[17] V.L. Kirillov, D.A. Balaev, S.V. Semenov, K.A. Shaikhutdinov, O.N. Martyanov, Mater. Chem. Phys. 145 (2014) 75.
[18] S. Mosivand, L.M.A. Monzon, K. Ackland, I. Kazeminezhad, J.M.D. Coey, J. Phys. D: Appl. Phys. 47 (2014), 055001.
[19] S. Mørup, D.E. Madsen, C. Fradsen, C.R.H. Bahl, M.F. Hansen, J. Phys.: Condens. Matter 19 (2007), 213202.
[20] Y.L. Raikher, V.I. Stepanov, J. Phys.: Condens. Matter. 20 (2008), 204120.
[21] S.A. Makhlouf, F.T. Parker, A.E. Berkowitz, Phys. Rev. B 55 (1997) R14717.
[22] J.G.E. Harris, J.E. Grimaldi, D.D. Awschalom, A. Chilero, D. Loss, Phys. Rev. B 60 (1999) 3513.
[23] M.S. Seehra, V.S. Babu, A. Manivannan, J.W. Lynn, Phys. Rev. B 61 (2000) 3513.
[24] C. Gilles, P. Bonville, H. Rakoto, J.M. Broto, K.K.W. Wong, S. Mann, J. Magn. Magn. Mater. 241 (2002) 430.
[25] A. Punnoose, T. Phanthavady, M.S. Seehra, N. Shah, G.P. Huffman, Phys. Rev. B 69 (2004), 054425.
[26] N.J.O. Silva, V.S. Amaral, L.D. Carlos, Phys. Rev. B 71 (2005), 184408.

[27] C.R.H. Bahl, M.F. Hansen, T. Pedersen, S. Saadi, K.H. Nielsen, B. Lebech, S. Mørup, J. Phys.: Condens. Matter 18 (2006) 4161–4175.
[28] D.A. Balaev, A.A. Dubrovskii, A.A. Krasikov, S.V. Stolyar, R.S. Iskhakov, V. P. Ladygina, E.D. Khilazheva, JETP Lett. 98 (3) (2013) 139.
[29] S.D. Tiwari, K.P. Rajeev, Solid State Commun. 152 (2012) 1080.
[30] C. Rani, S.D. Tiwari, J. Magn. Magn. Mater. 385 (2015) 272.
[31] S.I. Popkov, A.A. Krasikov, S.V. Semenov, A.A. Dubrovskii, S.S. Yakushkin, V.L. Kirillov, O.N. Mart'yanov, D.A. Balaev, Phys. Solid State, 62, (N9), 1518-1524 (2020).
[32] S.V. Stolyar, R.N. Yaroslavtsev, R.S. Iskhakov, O.A. Bayukov, D.A. Balaev, A. A. Dubrovskii, A.A. Krasikov, V.P. Ladygina, A.M. Vorotynov, M.N. Volochaev, Phys. Solid State 59 (2017) 555.
[33] D.A. Balaev, A.A. Dubrovskiy, A.A. Krasikov, S.I. Popkov, A.D. Balaev, K.A. Shaikhutdinov, V.L. Kirillov, and O. N. Mart'yanov, Phys. Solid State, 59, (N8), 1547 (2017).
[34] S.I. Popkov, A.A. Krasikov, A.A. Dubrovskiy, M.N. Volochaev, V.L. Kirillov, O. N. Martyanov, D.A. Balaev, J. Appl. Phys. 126 (2019), 103904.
[35] S.I. Popkov, A.A. Krasikov, D.A. Velikanov, V.L. Kirillov, O.N. Martyanov, D. A. Balaev, J. Magn. Magn. Mater. 483 (2019) 21.
[36] C. Parmar, G.S. Parmar, Supercond. Nov. Magn. 33 (2020) 441–444.
[37] L. Néel, C.R. Acad, Sci. Paris 252 (1961) 4075.
[38] R.H. Kodama, A.E. Berkowitz, E.J. McNiff, S. Foner, J. Appl. Phys. 81 (1997) 5552.
[39] R.H. Kodama, A.E. Berkowitz, Phys. Rev. **B** 59 (1999) 6321.
[40] Y.A. Koksharov, S.P. Gubin, I.D. Kosobudsky, G.Y. Yurkov, D.A. Pankratov, L. A. Ponomarenko, M.G. Mikheev, M. Beltran, Y. Khodorkovsky, A.M. Tishin, Phys. Rev. B 63 (2000), 012407.
[41] H. Khurshid, P. Lampen-Kelley, Ò. Iglesias, J. Alonso, M.-H. Phan, C.-J. Sun, M.-L. Saboungi, H. Srikanth, Sci. Rep. 5 (2015) 15054.
[42] B. Martínez, X. Obradors, Ll. Balcells, A. Rouanet, C. Monty, Phys. Rev. Lett. 80, 181–184 (1998).
[43] E. Winkler, R.D. Zysler, M. Vasquez Mansilla, D. Fiorani, D. Rinaldi, M. Vasilakaki, K.N. Trohidou, Nanotechnology 19 (2008), 185702.
[44] M.S. Seehra, V. Singh, X. Song, S. Bali, E.M. Eyring, J. Phys. Chem. Solids 71 (2010) 1362.
[45] N. Rinaldi-Montes, P. Gorria, D. Martínez-Blanco, A.B. Fuertes, L. Fernández Barquín, I. Puente-Orench, J.A. Blanco, Nanotechnology 26 (2015), 305705.
[46] M. Tadic, M. Panjan, D. Marković, I. Milošević, V. Spasojević, J. Alloy. Compd. 509 (2011) 7134.
[47] S.V. Stolyar, D.A. Balaev, V.P. Ladygina, A.I. Pankrats, R.N. Yaroslavtsev, D. A. Velikanov, R.S. Iskhakov, JETP Lett. 111 (2020) 183.
[48] E. Winkler, R.D. Zysler, M. Vasquez Mansilla, D. Fiorani, Phys. Rev. B 72 (2005), 132409.
[49] S.D. Tiwari, K.P. Rajeev, Phys. Rev. B 72 (2005), 104433.
[50] D. Martínez-Blanco, J.A. Pedro Gorria, M.J. Blanco, J.C. Pérez, Analysis of the diffraction-line broadening on nanostructured Fe: size–strain effects induced by milling and heating, Phys.: Condens. Matter. 20 (2008), 335213.
[51] R. Berger, J. Kliava, J.-C. Bissey, V. Baïetto, Magnetic resonance of superparamagnetic iron-containing nanoparticles in annealed glass, J. Appl. Phys. 87 (10) (2000) 7389–7396.
[52] R. Berger, J.-C. Bissey, J. Kliava, Lineshapes in magnetic resonance spectra, J. Phys.: Condens. Matter 12 (2000) 9347–9360.
[53] E.C. Stoner, E.P. Wohlfarth, Philos. Trans. Roy. Soc. Lond. Ser. A 240 (1948) 599.
[54] D.A. Balaev, A.A. Krasikov, A.A. Dubrovskiy, S.I. Popkov, S.V. Stolyar, O. A. Bayukov, R.S. Iskhakov, V.P. Ladygina, R.N. Yaroslavtsev, J. Magn. Magn. Mater. 410 (2016) 71.
[55] T. Iimor, Y. Imamoto, N. Uchida, Y. Kikuchi, K. Honda, T. Iwahashi, Y. Ouch, J. Appl. Phys. 127 (2020), 023902.
[56] C. Rani, S.D. Tiwari, Phys. B 513 (2017) 58.
[57] D.A. Balaev, S.I. Popkov, A.A. Krasikov, A.D. Balaev, A.A. Dubrovskiy, S.V. Stolyar, R.N. Yaroslavtsev, V.P. Ladygina, R.S. Iskhakov, Phys. Solid State 59 (2017) 1940.
[58] N.J.O. Silva, A. Millan, F. Palacio, E. Kampert, U. Zeitler, V.S. Amaral, Phys. Rev. B 79 (2009), 104405.
[59] L. Néel. C.R. Acad. Sci. Paris 253, 1286 (1961).
[60] L. Néel, C.R. Acad, Sci. Paris 253 (1961) 203.
[61] D.A. Balaev, A.A. Krasikov, A.A. Dubrovskiy, A.D. Balaev, S.I. Popkov, V.L. Kirillov, O.N. Martyanov, J. Supercond. Nov. Magn. 32 (2019) 405.
[62] A.D. Balaev, Y.V. Boyarshinov, M.M. Karpenko, B.P. Khrustalev, Prib. Tekh. Eksp. 3 (1985) 167.
[63] D.A. Velikanov, RF Patent No. 2481591C1, Byull. Izobret. No. 13 (2013). http://www.fips.ru/Archive/PAT/2013FULL/2013.05.10/DOC/RUNWC1/000/000/002/481/591/DOCUMENT.PDF.
[64] A.A. Bykov, S.I. Popkov, A.M. Parshin, A.A. Krasikov, Journal of Surface Investigation, X-ray, Synchrotron and Neutron Techniques 9 (2015) 111.
[65] E. Winkler, R.D. Zysler, D. Fiorani, Phys. Rev. B 70 (2004), 174406.
[66] X. Chen, S. Bedanta, O. Petracic, W. Kleemann, S. Sahoo, S. Cardoso, P.P. Freitas, Phys. Rev. B 72 (2005), 214436.
[67] A. Cabot, P. Alivisatos, W.F. Puntes, L. Balcells, O. Iglesias, A. Labarta, Phys. Rev. B 79 (2009), 094419.
[68] R.D. Desautels, E. Skoropata, Y.-Y. Chen, H. Ouyang, J.W. Freeland, J. Van Lierop, J. Phys.: Condens. Matter 24 (2012), 146001.
[69] D.A. Balaev, A.A. Krasikov, S.I. Popkov, A.A. Dubrovskiy, S.V. Semenov, D. A. Velikanov, V.L. Kirillov, O.N. Martyanov, J. Magn. Magn. Mater. 515 (2020), 167307.
[70] I. Sunagawa, Crystal growth – Its significance for modern science and technology and its possible future applications //Advances in Crystal Growth Research. – Elsevier Science BV, 2001. – p. 1-17. https://doi.org/10.1016/B978-044450747-1/50028-4.
[71] W.-L. Jang, Y.-M. Lu, W.-S. Hwang, T.-Li Hsiung, and H.P. Wang, Applied Physics Letters 94, 062103 (2009).
[72] D. Li, Z. Han, J.G. Zheng, X.L. Wang, D.Y. Geng, J. Li, Z.D. Zhang, Spin canting and spin-flop transition in antiferromagnetic Cr_2O_3 nanocrystals, J. Appl. Phys. 106 (5) (2009) 053913, https://doi.org/10.1063/1.3213100.
[73] R.D. Zysler, D. Fiorani, A.M. Testa, L. Suber, E. Agostinelli, M. Godinho, Size dependence of the spin-flop transition in hematite nanoparticles, Phys. Rev. B 68 (2003), 212408, https://doi.org/10.1103/PhysRevB.68.212408.
[74] O. Gomonay, S. Kondovych, V. Loktev, Shape-induced anisotropy in antiferromagnetic nanoparticles, J. Magn. Magn. Mater. 354 (2014) 125–135, https://doi.org/10.1016/j.jmmm.2013.11.003.
[75] F.L.A. Machado, P.R.T. Ribeiro, J. Holanda, R.L. Rodríguez-Suárez, A. Azevedo, S. M. Rezende, Phys. Rev. B 95 (2017), 104418.
[76] S. Thota, J.H. Shim, M.S. Seehra, J. Appl. Phys. 114 (2013), 214307.
[77] J. Wang, W. Wu, F. Zhao, G. Zhao, J. Appl. Phys. 109 (2011), 056101.
[78] X.G. Zheng, C.N. Xu, K. Nishikubo, K. Nishiyama, W. Higemoto, W.J. Moon, E. Tanaka, E.S. Otabe, Phys. Rev. B 72 (2005), 014464.
[79] A.E. Bianchi, S.J. Stewart, R.D. Zysler, G. Punte, J. Appl. Phys. 112 (2012), 083904.
[80] Yu.A. Kumzerov, N.F. Kartenko, L.S. Parfen'eva, I.A. Smirnov, A.A. Sysoeva, H. Misiorek, A. Jezowski, Phys. Solid State 54, 1066 (2012).
[81] N. Rinaldi-Montes, P. Gorria, D. Martínez-Blanco, A.B. Fuertes, I. Puente-Orench, L. Olivi, J.A. Blanco, AIP Adv. 6 (2016), 056104.
[82] M. Tadic, D. Nikolić, M. Panjan, G.R. Blake, J. Alloy. Compd. 647 (2015) 1061.
[83] V.P. Shilov, J.-C. Bacri, F. Gazeau, F. Gendron, R. Perzynski, Y.L. Raikher, J. Appl. Phys. 85 (1999) 6642.
[84] X. Batlle, A. Labarta, J. Phys. D: Appl. Phys. 35 (2002) R15.
[85] C.-R. Lin, R.-K. Chiang, J.-S. Wang, T.-W. Sung, J. Appl. Phys. 99 (2006) 08N710.
[86] D.A. Balaev, S.V. Semenov, A.A. Dubrovskiy, S.S. Yakushkin, V.L. Kirillov, O. N. Martyanov, J. Magn. Magn. Mater. 440 (2017) 199.
[87] Yu.V. Knyazev, D.A. Balaev, V.L. Kirillov, O.A. Bayukov, O.N. Mart'yanov, JETP Letters, 108, 527 (2018).
[88] I.G. Vazhenina, R.S. Iskhakov, L.A. Chekanova, Phys. Solid State 60 (2018) 292.
[89] J. Mohapatra, M. Xing, J. Elkins, J. Beatty, J Ping Liu, J. Phys. D: Appl. Phys. 53 (2020), 504004.
[90] D.A. Balaev, I.S. Poperechny, A.A. Krasikov, S.V. Semenov, S.I. Popkov, Y.V. Knyazev, V.L. Kirillov, S.S. Yakushkin, O.N. Martyanov, and Yu.L.. Raikher, J. Phys. D: Appl. Phys. 54, 275003 (2021). doi.org/10.1088/1361-6463/abf371.
[91] A. Aharoni, J. Appl. Phys. 61 (1987) 3302.
[92] F. Bødker, S. Mørup, S. Linderoth, Phys. Rev. Lett. 72 (1994) 282.
[93] E.L. Duarte, R. Itri, E. Lima Jr, M.S. Baptista, T.S. Berquó, G.F. Goya, Nanotechnology 17 (2006) 5549.
[94] T.S. Berquó, J.J. Erbs, A. Lindquist, R.L. Penn, S.K. Banerjee, J. Phys.: Condens. Matter. 21 (2009), 176005.
[95] Y.V. Knyazev, D.A. Balaev, S.V. Stolyar, O.A. Bayukov, R.N. Yaroslavtsev, V. P. Ladygina, D.A. Velikanov, R.S. Iskhakov, J. Alloy. Compd. 851 (2021), 156753.
[96] H. Shim, P. Dutta, M.S. Seehra, J. Bonevich, Solid State Commun. 145 (2008) 192–196.
[97] M.P. Proenca, C.T. Sousa, A.M. Pereira, P.B. Tavares, J. Ventura, M. Vazquez, J. P. Araujo, Phys. Chem. Chem. Phys. 13 (2011) 9561.
[98] D. Nikolić, M. Panjan, G.R. Blake, M. Tadic, J. Eur. Ceram. Soc. 35 (2015) 3843–3852.